

Prediction of Solar Irradiation in Africa using Linear-Nonlinear Hybrid Models

Youssef Kassem

Department of Mechanical Engineering, Engineering Faculty, Near East University, Cyprus | Energy, Environment, and Water Research Center, Near East University, Cyprus
yousseuf.kassem@neu.edu.tr (corresponding author)

Huseyin Camur

Department of Mechanical Engineering, Engineering Faculty, Near East University, Cyprus
huseyin.camur@neu.edu.tr

Mustapha Tanimu Adamu

Department of Mechanical Engineering, Engineering Faculty, Near East University, Cyprus
20215363@std.neu.edu.tr

Takudzwa Chikowero

Department of Mechanical Engineering, Engineering Faculty, Near East University, Cyprus
20215146@std.neu.edu.tr

Terry Apreala

Department of Mechanical Engineering, Engineering Faculty, Near East University, Cyprus
20224420@std.neu.edu.tr

Received: 18 June 2023 | Revised: 4 July 2023 | Accepted: 5 July 2023

Licensed under a CC-BY 4.0 license | Copyright (c) by the authors | DOI: <https://doi.org/10.48084/etasr.6131>

ABSTRACT

Solar irradiation prediction including Global Horizontal Irradiation (GHI) and Direct Normal Irradiation (DNI) is a useful technique for assessing the solar energy potential at specific locations. This study used five Artificial Neural Network (ANN) models and Multiple Linear Regression (MLR) to predict GHI and DNI in Africa. Additionally, a hybrid model combining MLR and ANNs was proposed to predict both GHI and DNI and improve the accuracy of individual ANN models. Solar radiation (GHI and DNI) and global meteorological data from 85 cities with different climatic conditions over Africa during 2001-2020 were used to train and test the models developed. The Pearson correlation coefficient was used to identify the most influential input variables to predict GHI and DNI. Two scenarios were proposed to achieve the goal, each with different input variables. The first scenario used influential input parameters, while the second incorporated geographical coordinates to assess their impact on solar radiation prediction accuracy. The results revealed that the suggested linear-nonlinear hybrid models outperformed all other models in terms of prediction accuracy. Moreover, the investigation revealed that geographical coordinates have a minimal impact on the prediction of solar radiation.

Keywords-global horizontal irradiation; direct normal irradiation; multiple linear regression; artificial neural networks; hybrid model

I. INTRODUCTION

The exploitation of fossil fuels faces increasing political and environmental challenges [1]. The use of renewable energy is one solution to address these issues and meet the growing global demand for electricity. Renewable energy offers a solution to the pollution and environmental damage caused by fossil and nuclear energy [2]. The potential of renewable

energy has inspired numerous researchers to explore clean technologies, intending to generate clean energy and minimize the effects of climate change [3-5]. Among the various renewable resources, solar energy is particularly promising, with applications in electricity generation, as well as air and water heating/cooling [6]. Solar photovoltaic (PV) energy generation uses solar modules that consist of multiple solar cells containing a PV material.

In general, assessing the energy generation potential for various solar technologies is based on two crucial parameters: Global Horizontal Irradiation (GHI) and Direct Normal Irradiation (DNI) [7]. Accurate measurement and prediction of GHI and DNI are crucial in assessing the energy generation potential of various solar technologies. These parameters are key inputs for designing, operating, and optimizing the performance of solar power plants. According to [8], GHI is the total amount of solar radiation received on a horizontal surface, including both direct and diffuse radiation. On the other hand, DNI is the amount of solar radiation received directly from the sun's rays, perpendicular to a surface. This type of radiation is particularly important for Concentrated Solar Power (CSP) plants that use mirrors or lenses to concentrate sunlight onto a receiver to produce high-temperature heat, which is then used to generate electricity [8]. Therefore, accurate and reliable measurements of GHI and DNI are essential for the effective operation and management of solar power plants in the future.

Recently, soft-computing approaches have emerged as particularly effective techniques for modeling global solar radiation in many regions around the world. Soft-computing techniques enable efficient identification of relationships between dependent and independent variables, even for non-linear natural processes. Recently, various models have been developed, such as Multilayer Feed-Forward Neural Networks, Support Vector Machines, Autoregressive Integrated Moving Averages, etc., that use different meteorological and geographical elements to estimate the total amount of solar radiation in terms of GHI and DNI [9-37]. Based on previous scientific studies [9-37], the most relevant input parameters used to predict solar radiation are average temperature, pressure, relative humidity, wind speed, wind direction, sunshine hours, minimum and maximum temperatures, wet-bulb temperature, atmospheric temperature, cloudiness, and evaporation.

Based on the above, various empirical models are used to estimate the annual amount of GHI and DNI in Africa, which is currently experiencing a major electricity crisis, with approximately 600 million people without access to electricity. Rural areas are particularly affected, with electrification rates as low as 10%. This energy poverty has significant negative impacts on the economy, society, and health, as communities rely on unsafe and inefficient energy sources. However, the abundant sunshine in Africa provides a unique opportunity for the development of solar energy systems, which have the potential to meet the energy needs of millions of people in the region. In this study, five ANN models (feed-forward neural network, cascade forward neural network, Elman neural network, Layer Recurrent Neural Network, and NARX Neural Network) and Multiple Linear Regression (MLR) were used to predict solar radiation data. Moreover, this study proposed linear-nonlinear hybrid models that integrate ANNs and MLR for GHI and DNI prediction. GHI, DNI, and global meteorological data from 85 cities in Africa with various climatic conditions were used to train and test the developed models. The Pearson correlation coefficient was used to identify the most influential input variables for predicting GHI and DNI. Two scenarios were used for this purpose: the first one was created using the most influential input parameters,

while the second incorporated geographical coordinates (latitude, longitude, and altitude) along with the influential input data to assess the impact of geographical coordinates on the accuracy of solar radiation prediction. Data were obtained from the NASA POWER dataset for the period 2000-2021.

II. MATERIAL AND METHODS

A. Study Area

Africa is a vast continent that spans the equator, and its climate varies greatly depending on the region. The continent includes several climatic zones, including tropical rainforest, savanna, and desert regions. The latitude and longitude of a region greatly influence its climate, which in turn affects weather patterns. The equator runs through the center of the continent, passing through countries. The weather in Africa can also be affected by various natural phenomena, such as the El Niño Southern Oscillation (ENSO), which is a climate cycle in the Pacific Ocean that affects global weather patterns. During El Niño, the Pacific Ocean warms, leading to changes in atmospheric pressure and wind patterns that affect rainfall patterns in Africa.

B. Data Used

The NASA POWER (Prediction Of Worldwide Energy Resource) dataset is a comprehensive collection of solar and meteorological data that provides information on various crucial parameters crucial for studying and analyzing renewable energy resources and their potential. The dataset covers locations around the world, allowing researchers and analysts to access solar and meteorological data for virtually any location on Earth. The NASA POWER dataset includes a wide range of parameters related to solar radiation and meteorological conditions. These data include solar radiation including GHI, DNI, Diffuse Horizontal Irradiance (DHI), and Clear Sky GHI, as well as meteorological data including temperature, relative humidity, wind speed, wind direction, precipitation, cloud cover, atmospheric pressure, and more. The dataset offers both hourly and daily temporal resolutions. Hourly data are available for certain parameters, allowing for a more detailed analysis of solar and meteorological conditions throughout the day. Daily data provide aggregated values for each parameter. The spatial resolution of the NASA POWER dataset varies depending on the specific parameter and the data source used. In general, the dataset provides information at a spatial resolution of approximately 1 km. The dataset integrates data from various sources, including satellite observations, ground measurements, and atmospheric models. NASA incorporates data from multiple sensors and instruments to provide accurate and reliable information. The NASA POWER dataset is freely accessible to the public through the NASA POWER web portal. Therefore, data including GHI, DNI, surface pressure, average, maximum, and minimum temperature, relative humidity, wind speed at 2 m height, average, maximum, and minimum wind speed at 10 m height, wind direction at 10 m height, frost point temperature, wet bulb temperature, cloud amount, and precipitation were collected for all the selected cities in Africa shown in Table I.

TABLE I. INFORMATION REGARDING THE SELECTED LOCATIONS

Location	Latitude [N°]	Longitude [E°]	Altitude [m]	Location	Latitude [N°]	Longitude [E°]	Altitude [m]
Cairo	30.0	31.6	350.0	Cabinda	-5.1	12.3	103.0
Kinshasa	-4.3	15.3	277.0	Fez	33.8	-4.9	971.0
Vereeniging	-26.6	27.9	1526.0	Uyo	5.0	7.9	71.0
Giza	30.0	31.2	19.0	Mwanza	-2.5	32.7	1134.0
Luanda	-9.5	13.5	201.0	Lilongwe	-14.0	33.7	1071.0
Dar es Salaam	-6.8	39.3	15.0	Kigali	-1.9	30.1	1575.0
Khartoum	15.6	32.5	387.0	Bukavu	-2.5	28.9	1533.0
Johannesburg	-26.2	28.1	1746.0	Abomey	6.4	2.3	30.0
Abidjan	5.4	-4.0	105.0	Nnewi	6.0	7.0	163.0
Alexandria	30.9	29.8	18.0	Tripoli	32.8	13.3	31.0
Addis Ababa	9.0	38.8	2315.0	Kaduna	10.4	7.9	661.0
Nairobi	-1.3	36.8	1657.0	Aba	5.1	7.4	64.0
Cape Town	-33.3	18.4	35.0	Bujumbura	-3.3	29.4	798.0
Yaoundé	3.9	11.5	715.0	Maputo	-26.0	32.6	14.0
Kano	12.0	8.5	454.0	Hargeisa	9.6	44.1	1267.0
East Rand	-26.4	27.4	1590.0	BoboDioulass	11.2	-4.3	420.0
Umuhia	5.5	7.5	154.0	Shubra el-Kheima	30.1	31.2	28.0
Douala	36.6	4.1	614.0	Ikorodu	6.6	3.5	36.0
Casablanca	33.3	-8.0	189.0	Asmara	15.3	38.9	2342.0
Ibadan	7.4	3.9	223.0	Marrakesh	31.6	-8.0	468.0
Antananarivo	19.0	46.7	1205.0	Tshikapa	-3.0	23.8	505.0
Abuja	9.1	7.5	473.0	Ilorin	8.5	4.5	318.0
Kampala	0.3	32.6	1237.0	Blantyre	-15.8	35.0	698.0
Kumasi	6.7	-1.6	260.0	Agadir	30.7	-9.6	454.0
Dakar	14.7	-17.3	6.0	Misratah	32.4	15.1	9.0
Port Harcourt	4.8	7.0	18.0	Lubumbashi	-11.7	27.5	1262.0
Durban	-29.9	31.0	13.0	Accra	5.8	0.1	39.0
Ouagadougou	12.4	-1.5	299.0	Brazzaville	-3.0	23.8	505.0
Lusaka	-15.4	29.2	1149.0	Monrovia	6.3	-10.8	6.0
Algiers	36.8	3.1	31.0	Tunis	33.8	9.4	43.0
Bamako	12.6	-8.0	335.0	Rabat	34.0	-6.8	87.0
Omdurman	15.6	32.5	391.0	Lomé	6.1	1.2	14.0
Mbuji-Mayi	-6.1	23.6	678.0	Benin City	6.3	5.6	90.0
Pretoria	-25.7	28.2	1338.0	Owerri	5.5	7.0	74.0
Kananga	-5.9	22.4	636.0	Warri	5.5	5.8	5.0
Harare	-17.9	31.1	1483.0	Jos	9.9	8.9	1182.0
Onitsha	6.1	6.8	51.0	Bangui	4.4	18.6	355.0
N'Djamena	12.1	15.1	297.0	Nampula	-15.1	39.3	430.0
Nouakchott	18.1	-16.0	8.0	Oran Algeria	35.6	-0.7	162.0
Mombasa	-4.0	39.7	10.0	West Rand	-26.2	27.5	1589.0
Niamey	13.5	2.1	207.0	Lubango	-14.9	13.5	1774.0
Pointe-Noire	-4.8	11.9	16.0	Gqeberha	-34.0	25.6	52.0

C. Artificial Neural Networks (ANNs)

ANNs are a class of machine learning algorithms inspired by the structure and functioning of biological neural networks, such as the human brain [38]. An ANN consists of interconnected nodes, called artificial neurons or "nodes," organized into layers. The three main types in an ANN are the input, hidden, and output. The connections between neurons in an ANN are represented by weights. During the training process, the weights are adjusted based on a mathematical optimization algorithm, such as gradient descent, to minimize the difference between the predicted and desired outputs. This adjustment is performed through a process called backpropagation, in which the error is propagated backward through the network to update the weights.

Activation functions play a crucial role in determining the output of a neuron based on the weighted inputs. The most common activation functions are logistic-sigmoid (*logsig*) and

tangent-sigmoid (*tansig*) whose outputs lie between 0 and 1 and are defined as [38]:

$$\text{logsig} = \frac{1}{1+e^{-x}} \quad (1)$$

$$\text{tansig} = \frac{e^x - e^{-x}}{e^x + e^{-x}} \quad (2)$$

In addition, a trial-and-error approach is typically employed to determine the optimal number of nodes in the hidden layer. This study used the TRAINLM training function, which updates the weights and biases of neuron connections based on the Levenberg-Marquardt (LM) optimization algorithm. The backpropagation algorithm, a type of gradient descent algorithm, serves as the learning algorithm for this purpose. The training process of an ANN is crucial, involving the adjustment of weights and biases to minimize the disparity between the ANN's output and the desired values. The Mean Squared Error (MSE) is used to optimize the performance of the trained ANN model, which quantifies the average squared

difference between the predicted and actual values, serving as a measure to guide the training procedure toward better accuracy. Figure 1 illustrates the schematic representation of the ANN model developed to predict the GHI and DNI.

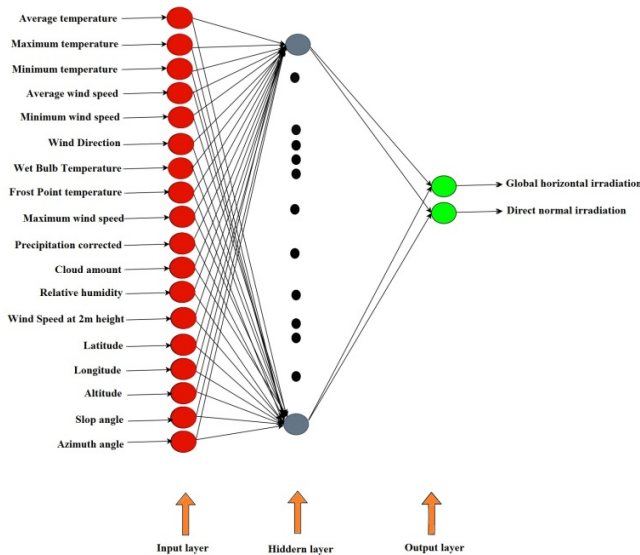


Fig. 1. Schematic representation of the ANN model used.

1) Feed-Forward Neural Network (FFNN)

FFNN is widely used in various domains to analyze different types of problems in different scenarios [38-40]. The Levenberg-Marquardt algorithm and the backpropagation method are commonly used techniques [40]. The trial and error method is used to determine the appropriate number of hidden layers and neurons, and MSE is used to assess the performance of the training algorithm. It is important to note that the data were normalized within the range of 0-1. This study used the backpropagation algorithm for the training process.

2) Cascade Feed-Forward Neural Network (CFNN)

CFNN is conceptually similar to the FFNN [40-42] and consists of three types of layers: an input layer, one or more hidden layers, and an output layer. The input layer receives weights from the input data [38-40]. Each subsequent layer receives weights from the input layer and all preceding layers [38-40]. Biases are present in all layers, contributing to the network's functionality. The final layer corresponds to the output layer. The configuration of weights and biases is necessary for each layer. During the training phase, MSE is computed to assess the model's performance.

3) Elman Neural Network (ENN)

ENN is a feedback neural network known for its exceptional computational capabilities [39-40], and consists of four layers, namely, the input, hidden, context, and output layers [39-40]. The input layer functions as the signal transmission component, while the output layer has a linear weight effect. The distinguishing feature of ENN compared to backpropagation neural networks is the inclusion of the context layer [39-40].

4) Layer Recurrent Neural Network (LRNN)

LRNN incorporates recurrent connections at the layer level [41]. In traditional RNNs, such as the Elman or Jordan architectures, the recurrent connections are typically at the neuron level. However, in LRNN, recurrent connections are established between entire layers of neurons, and each layer is associated with a recurrent connection that allows information to flow from the previous to the current time step within the same layer [41]. This enables the network to capture and utilize temporal dependencies in sequential data. Recurrent connections in LRNN can improve the model's ability to process and analyze time series or sequential data, making it particularly suitable for tasks such as speech recognition, language modeling, and music generation, where capturing long-term dependencies is crucial. By incorporating layer-level recurrent connections, LRNN provides an alternative approach to modeling sequential data compared to traditional recurrent architectures. Its unique structure allows the efficient processing of temporal information and can lead to improved performance in tasks that involve sequential data analysis.

5) Nonlinear Autoregressive Network with Exogenous Input (NARX)

NARX combines autoregressive elements with exogenous input to predict future values of a time series [42]. It is designed to capture nonlinear dependencies and patterns in time series data, incorporating both the past values of the target series (autoregressive component) and external factors or inputs that may influence the target series (exogenous component). NARX typically consists of an input layer, one or more hidden layers, and an output layer. The input layer receives both the past values of the target series (autoregressive inputs) and any exogenous inputs that may be available. The hidden layers process the input information and learn to capture the nonlinear relationships and dynamics of the data. Finally, the output layer generates the predicted values of the target series. An important aspect of the NARX model is the use of time-delayed inputs, where past values of the target series and exogenous inputs are fed as input features with a time delay. The model can consider historical information and dependencies between past and future observations by including these time-delayed inputs. Training the NARX model typically involves using optimization algorithms, such as gradient descent, to adjust its weights and biases to minimize prediction errors. The performance of the NARX model can be evaluated using MSE or Root Mean Squared Error (RMSE). NARX has been used in various domains, including finance, economics, weather forecasting, and time series prediction tasks in general. Its ability to capture nonlinear relationships and incorporate exogenous factors makes it a powerful tool for modeling and predicting complex time-series data.

D. Multiple Linear Regression (MLR)

MLR is a statistical method to analyze the relationship between a dependent variable and multiple independent variables. It extends the concept of simple linear regression by considering multiple predictors simultaneously. In MLR, the goal is to create a linear equation that best fits the relationship between the dependent and independent variables.

E. Hybrid Modeling (HM)

HM is a valuable technique for capturing different parts of the underlying patterns by combining several models [43]. In this study, an HM was developed by combining the predicted values of MLR and estimated residuals (error) by a nonlinear model (computational models). Three steps were taken in the development of HM:

- Step 1: Estimate the properties using the mathematical models and determine the residuals.
- Step 2: Pass the residual through computational models to capture the nonlinearity of the data.
- Step 3: Combine the obtained output from the mathematical and computational models to predict fuel properties.

F. Statistical Indices

The performance evaluation of the developed models involves the utilization of several statistical metrics. This study used the Coefficient of Determination (R^2), RMSE, and Mean Absolute Error (MAE). Equations (3)-(5) present the mathematical expressions for these metrics.

$$R^2 = 1 - \frac{\sum_{i=1}^n (a_{a,i} - a_{p,i})^2}{\sum_{i=1}^n (a_{p,i} - a_{a,ave})^2} \tag{3}$$

$$RMSE = \sqrt{\frac{1}{n} \sum_{i=1}^n (a_{a,i} - a_{p,i})^2} \tag{4}$$

$$MAE = \frac{1}{n} \sum_{i=1}^n |a_{a,i} - a_{p,i}| \tag{5}$$

TABLE II. DESCRIPTIVE STATISTICS OF THE USED DATA

City	DNI (kWh/m ²)	Class	GHI (kWh/m ²)	Class	City	DNI (kWh/m ²)	Class	GHI (kWh/m ²)	Class
Aba	929	1 (poor)	1650	4 (good)	Kigali	1142	2 (marginal)	1804	4 (good)
Abdijan	1004	2 (marginal)	1707	4 (good)	Kinshasa	1002	2 (marginal)	1640	4 (good)
Abomey Calavi	1013	2 (marginal)	1692	4 (good)	Kumasi	1023	2 (marginal)	1713	4 (good)
Abuja	1321	3 (fair)	1918	5 (excellent)	Libreville	847	1 (poor)	1568	4 (good)
Accra	1254	2 (marginal)	1849	5 (excellent)	Lilongwe	1718	4 (good)	2010	5 (excellent)
Addis Ababa	2111	5 (excellent)	2128	5 (excellent)	Lokoja	1080	2 (marginal)	1762	4 (good)
Agadir	2196	6 (outstanding)	2072	5 (excellent)	Lome	1091	2 (marginal)	1764	4 (good)
Alexandria	2111	5 (excellent)	2128	5 (excellent)	Luanda	1215	2 (marginal)	1752	4 (good)
Algiers	1756	4 (good)	1749	4 (good)	Lubango	2206	6 (outstanding)	2206	6 (outstanding)
Antananarivo	2086	5 (excellent)	2146	5 (Excellent)	Lubumbashi	1842	5 (excellent)	2082	5 (excellent)
Asmara	2027	5 (excellent)	2236	6 (outstanding)	Lusaka	2401	6 (outstanding)	2223	6 (outstanding)
Bamako	1754	4 (good)	2131	5 (excellent)	Maiduguri	1707	4 (good)	2153	6 (outstanding)
Bangui	1261	3 (fair)	1860	5 (excellent)	Maputo	1806	4 (good)	1833	4 (good)
Benguela	1866	5 (excellent)	2051	5 (excellent)	Marrakesh	2367	6 (outstanding)	2062	5 (excellent)
Benin City	914	1 (poor)	1625	4 (good)	Mbuji-Mayi	1330	3 (fair)	1865	5 (excellent)
Blantyre	1716	4 (good)	1994	5 (Excellent)	Misratah	1777	4 (good)	1863	5 (excellent)
Bobo Dioulasso	1658	4 (good)	2156	6 (outstanding)	Mombasa	1717	4 (good)	2067	5 (excellent)
Brazzaville	1023	2 (marginal)	1710	4 (good)	Monrovia	992	2 (marginal)	1665	4 (good)
Bujumbura	1184	2 (marginal)	1802	4 (good)	Mwanza	1577	4 (good)	1999	5 (excellent)
Bukavu	1075	2 (marginal)	1740	4 (good)	Nairobi	1761	4 (good)	2116	5 (excellent)
Cabinda	841	1 (poor)	1507	3 (fair)	Nampula	1745	4 (good)	2053	5 (excellent)
Cairo	2084	5 (excellent)	2083	5 (excellent)	Ndjamena	1849	5 (excellent)	2227	6 (outstanding)
Cape Town	2516	6 (outstanding)	2025	5 (excellent)	Niamey	1806	4 (good)	2204	6 (outstanding)
Casablanca	1897	5 (excellent)	1891	5 (excellent)	Nnewi	899	1 (poor)	1613	4 (good)
Dakar	1589	4 (good)	2099	5 (excellent)	Nouakchott	1917	5 (excellent)	2289	6 (outstanding)
Dar es Salam	1750	4 (good)	2062	5 (excellent)	Omdurman	2423	6 (outstanding)	2405	6 (outstanding)
Doula	852	1 (poor)	1554	4 (good)	Onitsha	955	2 (marginal)	1665	4 (good)
Durban	1679	4 (good)	1706	4 (good)	Oran	1813	4 (good)	1807	4 (good)
East rand	992	2 (marginal)	1016	1 (poor)	Ouagadougou	1690	4 (good)	2119	5 (excellent)
Enugu	1019	2 (marginal)	1722	4 (good)	Owerri	929	1 (poor)	1650	4 (good)
Fez	2094	5 (excellent)	1956	5 (excellent)	Point-Noire	902	1 (poor)	1555	4 (good)
Giza	1005	2 (marginal)	1676	4 (good)	Port Harcourt	834	1 (poor)	1504	3 (fair)
Gqeberha	2124	5 (excellent)	1827	4 (good)	Pretoria	2323	6 (outstanding)	2070	5 (excellent)
Harare	2029	5 (excellent)	2117	5 (excellent)	Rabat	2197	6 (outstanding)	1965	5 (excellent)
Hargeisa	2460	6 (outstanding)	2442	6 (outstanding)	Shubra el-Kheima	2084	5 (excellent)	2083	5 (excellent)
Ibadan	982	2 (marginal)	1676	4 (good)	Tangier	1935	5 (excellent)	1801	4 (good)
Ikorodu	1005	2 (marginal)	1676	4 (good)	Tripoli	1856	5 (excellent)	1970	5 (excellent)
Ilorin	1182	2 (marginal)	1824	4 (good)	Tshikapa	1022	2 (marginal)	1681	4 (good)
Johannesburg	2224	6 (outstanding)	2030	5 (excellent)	Tunis	2174	5 (excellent)	2038	5 (excellent)
Jos	1335	3 (fair)	1930	5 (excellent)	Umuahia	929	1 (poor)	1650	4 (good)
Kaduna	1510	3 (fair)	2038	5 (excellent)	Uyo	929	1 (poor)	1650	4 (good)
Kampala	1309	3 (fair)	1932	5 (excellent)	Vereeniging	2303	6 (outstanding)	2057	5 (excellent)
Kananga	1164	2 (marginal)	1779	4 (good)	Warri	809	1 (poor)	1555	4 (good)
Kano	1615	4 (good)	2126	5 (Excellent)	West rand	2303	6 (outstanding)	2057	5 (excellent)
Khartoum	2423	6 (outstanding)	2405	6 (outstanding)	Yaounde	856	1 (poor)	1633	4 (good)

III. RESULTS AND DISCUSSION

A. Solar Energy Characteristics

The classification of the solar energy potential was determined considering the annual GHI and DNI values. The classification of solar resources can be found in [44]. Table II presents the classification of solar resources in a specific city based on GHI and DNI values. Based on the annual value of GHI, it is observed that most of the selected regions exhibit abundant solar resources and are classified into good, excellent, and outstanding categories. Furthermore, solar resources in the East are classified as poor (class 1). Moreover, it is noticed that the solar resources in Cabinda and Port Harcourt are categorized as fair (class 3). Consequently, these regions emerge as the most favorable locations for the future installation of PV systems, primarily due to their significantly high GSR values.

Based on the annual value of the DNI, solar resources in 14% of the selected regions were classified as outstanding (Class 6). These regions are Agadir, Rabat, Lubango, Johannesburg, Vereeniging, West Rand, Pretoria, Marrakesh, Lusaka, Khartoum, Omdurman, Hargeisa, and Cape Town. Furthermore, solar resources in 14% of the selected regions

(Warri, Port Harcourt, Cabinda, Libreville, Doula, Yaounde, Nnewi, Point-Noire, Benin City, Aba, Owerri, Umuahia, and Uyo) were classified as poor (Class 1). Consequently, based on the high values of GHI and DNI, it can be concluded that most of the selected locations are well-suited for the installation of both large- and small-scale PV systems. Moreover, these regions are also highly suitable for implementing flat-plate PV systems and CSP systems.

B. Selecting Relevant Parameters

The evaluation of the solar potential of a specific location is a crucial initial step in the effective planning of solar energy systems. Additionally, the prediction of solar radiation is influenced by various meteorological and geographical variables, making the identification of appropriate factors for accurate solar radiation prediction a significant area of research. According to [45], accurate information about the specific amount of solar energy available at a particular geographical location during a given period is essential and plays a vital role in the design process of PV systems. Moreover, meteorological parameters play a pivotal role in influencing the amount of solar radiation [46-47]. Furthermore, the orientation angles of a PV system have a significant impact on its performance [48-49].

TABLE III. PEARSON CORRELATION MATRIX FOR INPUT AND OUTPUT PARAMETERS

GHI																	
	SI	Az	SP	Tav	RH	WS-2	WD	WS	FPT	WPT	Tmax	Tmin	CA	WSmax	WSmin	PC	GHI
SI	1																
Az	-0.1	1															
SP	-0.13	0.49	1														
Tav	-0.26	0.457	0.364	1													
RH	-0.27	0.076	0.315	-0.01	1												
WS-2	0.161	-0.15	0.219	-0.29	-0.26	1											
WD	0.023	0.24	0.312	-0.12	0.091	0.116	1										
WS	0.185	-0.19	0.171	-0.33	-0.33	0.988	0.084	1									
FPT	-0.36	0.283	0.451	0.514	0.845	-0.36	0.018	-0.44	1								
WPT	-0.37	0.398	0.476	0.797	0.589	-0.38	-0.04	-0.45	0.928	1							
Tmax	0.225	0.244	0.062	0.218	-0.76	0.034	0.032	0.09	-0.53	-0.28	1						
Tmin	-0.38	0.277	0.396	0.732	0.557	-0.23	-0.1	-0.32	0.869	0.93	-0.38	1					
CA	-0.24	0.089	0.014	0.278	0.677	-0.63	-0.19	-0.67	0.701	0.614	-0.56	0.587	1				
WSmax	0.287	-0.22	0.038	-0.57	-0.37	0.822	0.079	0.852	-0.6	-0.67	0.178	-0.6	-0.67	1			
WSmin	-0.03	-0.09	0.158	0.011	-0.02	0.377	0.043	0.374	0	0.005	-0.04	0.069	-0.19	0.173	1		
PC	-0.27	0.104	0.03	0.266	0.642	-0.58	-0.15	-0.61	0.661	0.581	-0.48	0.502	0.732	-0.601	-0.159	1	
GHI	0.162	-0.11	-0.36	0.013	-0.79	0.402	-0.08	0.444	-0.64	-0.45	0.557	-0.38	-0.76	0.385	0.123	-0.56	1
DNI																	
	SI	Az	SP	Tav	RH	WS-2	WD	WS	FPT	WPT	Tmax	Tmin	CA	WSmax	WSmin	PC	DNI
SI	1																
Az	-0.1	1															
SP	-0.13	0.49	1														
Tav	-0.26	0.457	0.364	1													
RH	-0.27	0.076	0.315	-0.01	1												
WS-2	0.161	-0.15	0.219	-0.29	-0.26	1											
WD	0.023	0.24	0.312	-0.12	0.091	0.116	1										
WS	0.185	-0.19	0.171	-0.33	-0.33	0.988	0.084	1									
FPT	-0.36	0.283	0.451	0.514	0.845	-0.36	0.018	-0.44	1								
WPT	-0.37	0.398	0.476	0.797	0.589	-0.38	-0.04	-0.45	0.928	1							
Tmax	0.225	0.244	0.062	0.218	-0.76	0.034	0.032	0.09	-0.53	-0.28	1						
Tmin	-0.38	0.277	0.396	0.732	0.557	-0.23	-0.1	-0.32	0.869	0.93	-0.38	1					
CA	-0.24	0.089	0.014	0.278	0.677	-0.63	-0.19	-0.67	0.701	0.614	-0.56	0.587	1				
WSmax	0.287	-0.22	0.038	-0.57	-0.37	0.822	0.079	0.852	-0.6	-0.67	0.178	-0.6	-0.67	1			
WSmin	-0.03	-0.09	0.158	0.011	-0.02	0.377	0.043	0.374	0	0.005	-0.04	0.069	-0.19	0.173	1		
PC	-0.27	0.104	0.03	0.266	0.642	-0.58	-0.15	-0.61	0.661	0.581	-0.48	0.502	0.732	-0.601	-0.159	1	
DNI	0.289	-0.29	-0.27	-0.42	-0.72	0.586	0.083	0.637	-0.81	-0.76	0.477	-0.69	-0.92	0.7	0.129	-0.69	1

This study used Pearson’s correlation to identify the most influential input among potential variables. Based on the Pearson coefficient, the strength of the relationships can be categorized as follows [50]: 0.00–0.25 indicates a very weak relationship, 0.26–0.49 represents a weak relationship, 0.50–0.69 corresponds to a moderate relationship, 0.70–0.89 signifies a strong relationship and 0.90–1.0 denotes a very strong relationship. Table III lists the Pearson correlation matrix depicting the relationships between the potential input parameters and the failure modes. The matrix provides an overview of the correlation coefficients between these variables. This study investigated the influence of geographical coordinates on the accuracy of the prediction of GHI and DNI. To achieve this objective, the proposed models were implemented and evaluated in two different scenarios, as shown in Figure 2. Different empirical models were used to predict the annual value of GHI and DNI. In general, data partitioning can influence model performance [51]. Moreover, in [51], it was concluded that empirical models achieve optimal performance when approximately 70-80% of the data are allocated for training and the remaining 20-30% are set aside for testing purposes. Consequently, the data were divided into training and testing sets using an arbitrary approach, with 80% of the total data assigned to the training set and the remaining 20% designated for the testing set. Table IV displays the descriptive statistics for the selected data.

C. Results of ANN models

An iterative algorithm was used to find the best neural network model and determine the optimal combination of input variables and hidden layer neurons. The study considered a range of 1-10 hidden layers and 10000-1000000 trial iterations. The Levenberg-Marquardt training algorithm was selected for its speed and reliability. Each network was trained multiple times to prevent inaccurate estimates. The model with the lowest MSE was chosen as the best-trained model. Table V presents the optimal network structure and activation function. The performance evaluation of the developed models was performed using R², RMSE, and MAE. Table VI presents the values of these statistical indexes for all proposed ANN models, and the following can be concluded:

- For GHI prediction, it is noticed that the FFNN model had the highest R² value compared to other models. On the other hand, the LRNN model had the lowest RMSE and MAE values, indicating superior performance compared to the other models. As shown in Table VI, the accuracy of GHI prediction was reduced when the geographical coordinates Lat, Long, and Alt were used as input variables for the models.
- For DNI prediction, it was found that the FFNN model exhibited the highest R² value among all models, indicating its superiority. Besides, the ENN model demonstrated the lowest RMSE and MAE values, suggesting superior performance compared to the others. The results showed that the accuracy of the DNI prediction increased when geographic coordinates were used as input variables.

TABLE IV. DESCRIPTIVE STATISTICS OF THE USED DATA

Data	Variable	Unit	Mean	SD	Min.	Max.
Training	Lat.	°	3.6	17.0	-34.0	36.8
	Long	°	16.4	15.8	-17.3	46.7
	Alt.	m	555.7	597.6	6.0	2342.0
	Sl.	°	17.7	15.7	-1.0	90.0
	Az.	°	-54.4	81.8	-180.0	47.0
	SP	kPa	96.1	5.6	81.4	101.7
	Tav	°C	23.6	3.6	8.4	30.1
	RH	%	68.8	15.2	23.8	89.2
	WS-2m	m/s	2.4	1.1	0.5	6.1
	WD	°	195.2	94.2	0.4	359.5
	WS	m/s	3.4	1.2	1.0	7.2
	FPT	°C	16.0	5.6	4.1	24.3
	WBT	°C	19.8	3.9	7.2	25.7
	Tmax	°C	36.5	4.9	25.3	46.9
	Tmin	°C	11.9	5.9	-8.7	23.5
	CA	%	54.4	15.9	11.4	86.9
	WSmax	m/s	10.1	3.6	2.8	22.9
	WSmin	m/s	0.1	0.1	0.0	1.4
	PC	mm/day	2.8	1.9	0.0	20.3
	DNI	kWh/m ² /day	4.3	1.4	2.0	7.7
GHI	kWh/m ² /day	5.3	0.7	2.6	6.8	
Testing	Lat.	°	8.8	20.9	-26.6	35.6
	Long	°	11.4	11.6	-6.8	31.2
	Alt.	m	403.9	528.1	5.0	1589.0
	Sl.	°	19.8	11.4	0.0	34.0
	Az.	°	-27.2	67.2	-179.0	18.0
	SP	kPa	97.2	5.2	84.7	101.6
	Tav	°C	22.4	3.4	15.8	28.6
	RH	%	70.8	15.6	39.3	90.3
	WS-2m	m/s	2.0	1.0	0.1	4.4
	WD	°	228.7	101.0	0.9	360.0
	Wsav	m/s	3.0	1.1	0.7	5.3
	FPT	°C	15.6	6.8	4.5	24.1
	WPT	°C	19.0	4.9	10.8	25.0
	Tmax	°C	37.0	4.8	29.1	47.8
	Tmin	°C	8.9	7.8	-6.2	21.2
	CA	%	54.3	18.9	22.8	84.6
	Wsmax	m/s	9.9	4.4	1.7	20.9
	Wsmmin	m/s	0.1	0.1	0.0	0.5
	PC	mm/day	3.0	2.3	0.0	11.0
	DNI	kWh/m ² /day	4.2	1.7	1.8	7.1
GHI	kWh/m ² /day	5.0	0.6	4.0	6.0	

SD: Standard deviation; Min.: Minimum; Max.: Maximum

TABLE V. BEST NETWORK STRUCTURE BASED ON THE TRAINING SET FOR HORIZONTAL SOLAR RADIATION

Model	Scenario	Number of hidden layers	Number of neurons	Transfer function
FFNN	1	2	5	tansig
	2	1	15	tansig
ENN	1	2	10	logsig
	2	2	10	tansig
CFNN	1	1	15	logsig
	2	1	5	tansig
LRNN	1	2	5	tansig
	2	2	15	tansig
NARX	1	2	15	logsig
	2	1	5	tansig

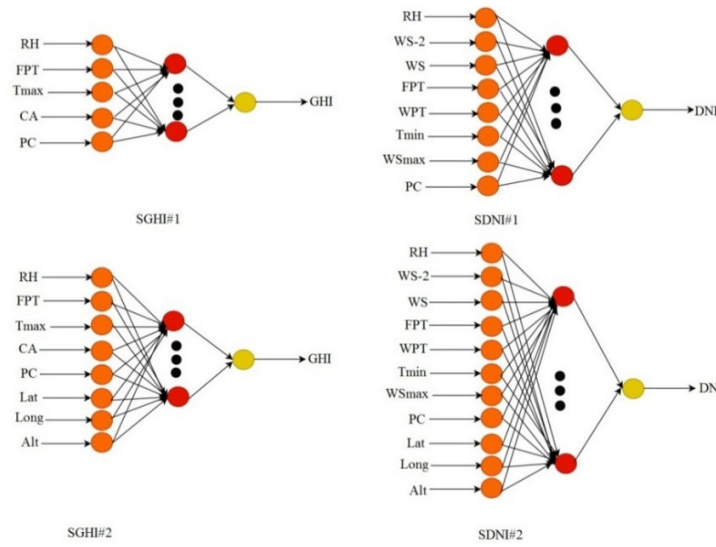


Fig. 2. Model development for predicting GHI and DNI considering the two scenarios.

TABLE VI. STATISTICAL INDEXES AND SCENARIO USED FOR ALL PROPOSED ANN MODELS IN TESTING

Output	Scenario	Variable	FFNN	LRNN	CFNN	ENN	NARX
GHI	SGHI#1	R ²	0.8287	0.5404	0.8278	0.7986	0.7858
		RMSE	0.4386	0.3976	0.4125	0.4144	0.3537
		MAE	0.3826	0.3073	0.3438	0.3276	0.2472
	SGHI#2	R ²	0.8154	0.7657	0.5637	0.8263	0.6443
		RMSE	0.3226	0.4102	0.3920	0.6104	0.4080
		MAE	0.2711	0.3414	0.3283	0.5434	0.3029
DNI	SDNI#1	R ²	0.9232	0.4533	0.9095	0.9047	0.9105
		RMSE	0.5975	1.5089	0.6266	0.5340	0.6725
		MAE	0.4354	1.0055	0.4458	0.3837	0.4945
	SDNI#2	R ²	0.8862	0.4739	0.9249	0.8987	0.8650
		RMSE	0.6694	1.4296	0.7061	0.5902	0.6720
		MAE	0.5243	0.9555	0.5563	0.4505	0.5075

RMSE and MAE are in kWh/m²

D. Results of MLR

MLR was used to predict the GHI and DNI in Africa. The training data were used to derive mathematical equations, represented by the following equations for the two scenarios:

$$GHI = 8.562 - 0.035 \cdot RH + 0.021 \cdot FPT - 0.018 \cdot Tmax - 0.014 \cdot CA + 0.012 \cdot PC \quad (6)$$

$$GHI = 9.172 - 0.049 \cdot RH + 0.074 \cdot FPT - 0.034 \cdot Tmax - 0.017 \cdot CA + 0.018 \cdot PC + 0.011 \cdot Lat + 0.001 \cdot Long \quad (7)$$

$$DNI = 8.911 - 0.015 \cdot RH + 1.533 \cdot WS_{2m} - 1.46 \cdot WS - 0.188 \cdot FPT - 0.016 \cdot Tmin + 0.061 \cdot WS_{MAX} + 0.034 \cdot PC \quad (8)$$

$$DNI = 11.092 - 0.008 \cdot RH + 2.113 \cdot WS_{2m} - 2.078 \cdot WS - 0.268 \cdot FPT - 0.022 \cdot Tmin + 0.038 \cdot WS_{MAX} + 0.06 \cdot PC - 0.011 \cdot lat - 0.014 \cdot Long - 0.001 \cdot Alt \quad (9)$$

Figures 3 and 4 present the time series plots of the observed and predicted GHI and DNI values for the two scenarios in the testing phase, using ANNs and MLR, respectively.

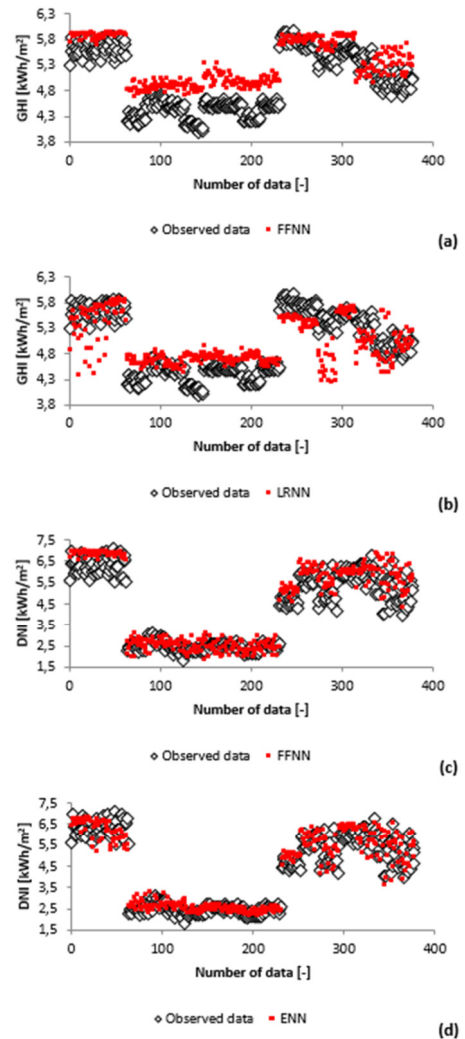


Fig. 3. Time series and the scatter of observed and predicted GHI (a), (b) and DNI (c), (d) for best scenario using ANN models.

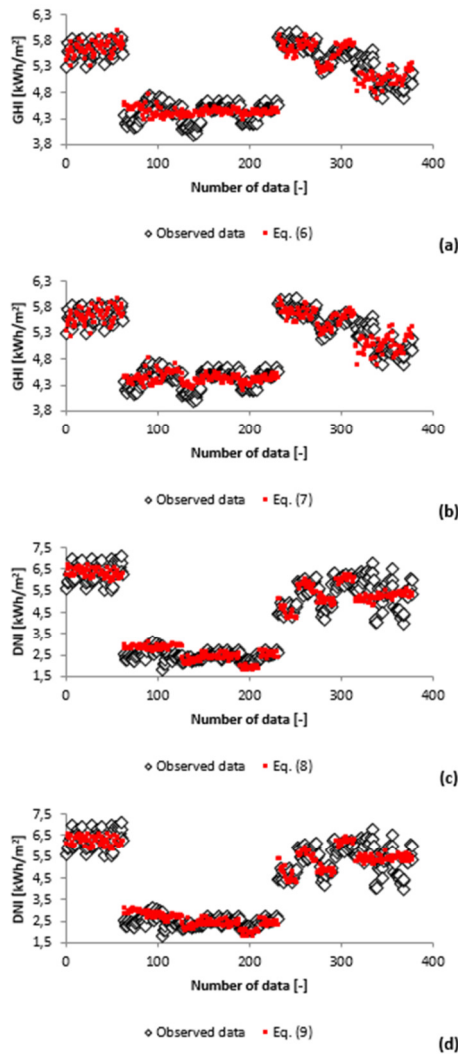


Fig. 4. Time series and the scatter of observed and predicted GHI (a), (b) and DNI (c), (d) using MLR.

The results demonstrate that incorporating Latitude, Longitude, and Altitude as input variables in the models improved the predictive accuracy of GHI and DNI by 1.67% and 0.78%, respectively.

E. Results of the Hybrid Models

An HM refers to combining multiple types of techniques to improve the prediction accuracy of a single model (FFNN, ENN, CFNN, LRNN, NARX, and MLR). Figures 5 and 6 show that the HMs outperformed the others in terms of data fit. This implies that the HMs provide a better fit to the observed data compared to the single ANN models. Figure 5 shows that the ENN-MLR (SGHI#2) model achieved a notably higher R^2 value compared to other models. Figure 6 shows that the CFNN-MLR (SDNI#2) produced a high R^2 value compared to the other models. Figure 7 shows time series plots of the observed and predicted GHI and DNI values for the testing phase. The ENN-MLR (SGHI#2) and CFNN-MLR (SDNI#2) models demonstrated a stronger correlation and better overall fit to the data.

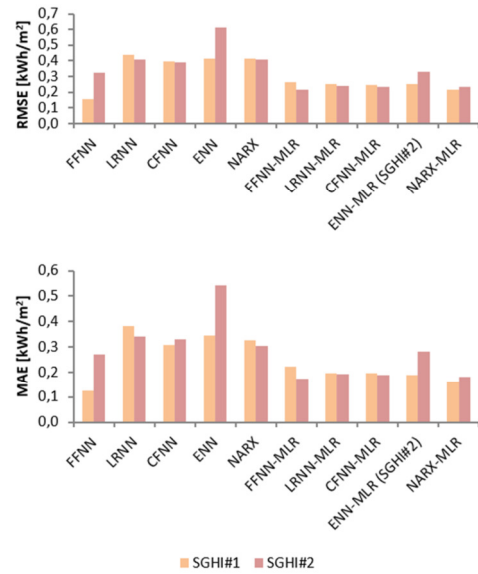


Fig. 5. RMSE and MAE for HM and single ANN models for predicting GHI.

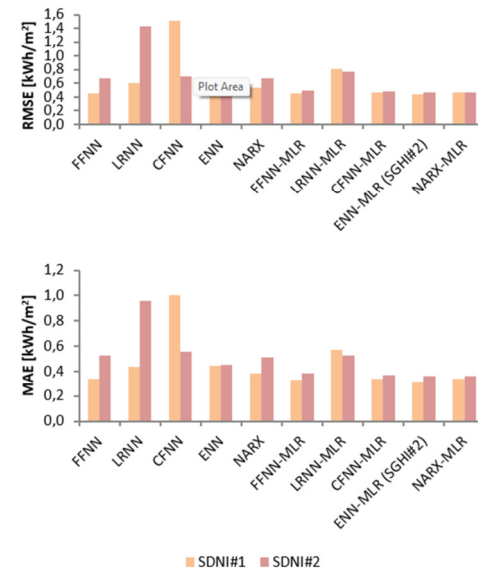


Fig. 6. RMSE and MAE for HM and single ANN models for predicting DNI.

IV. DISCUSSION AND CONCLUSION

Accurate predictions of solar radiation, including GHI and DNI, are vital for sizing, estimating energy production, monitoring performance, selecting optimal sites, and facilitating grid integration of solar systems. These predictions enable efficient planning, optimal utilization of solar resources, and the successful implementation of solar energy projects. According to [52], accurate solar radiation predictions help to determine the appropriate size and capacity of solar systems. Furthermore, considering the GHI and DNI values along with other factors such as panel efficiency and system losses, it is possible to forecast the expected energy output [9, 53]. Furthermore, solar radiation measurements and predictions

allow for the continuous monitoring of the performance of a solar system [54]. Additionally, accurate solar radiation predictions are essential for effectively integrating solar energy into the grid [55].

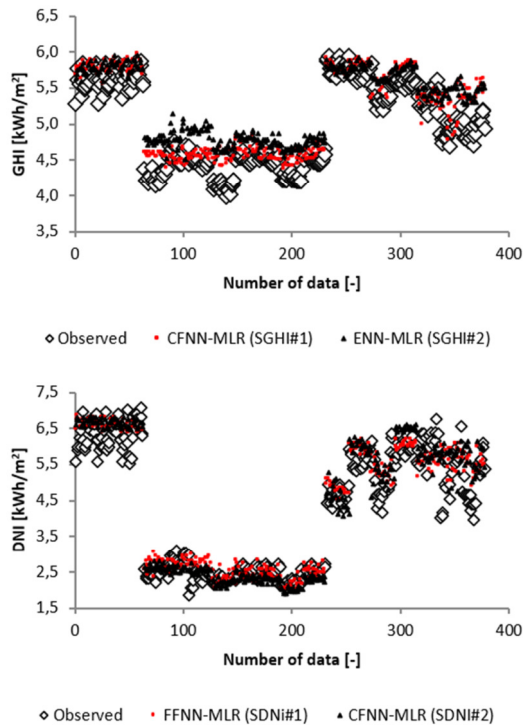


Fig. 7. Time series and the scatter of observed and predicted GHI and DNI values using HMs.

The performance of 11 empirical models was evaluated for the prediction of GHI and DNI. Solar radiation data, including GHI and DNI, from 85 cities having different climatic conditions all over Africa during 2001-2020 were used for training and testing. Based on the performance indexes, the proposed linear-nonlinear hybrid models exhibited superior performance in terms of predicting accuracy compared to all the other models considered. Furthermore, the results showed that geographical coordinates have a minimal impact on the prediction of solar radiation, as also supported in other studies. In [46], it was found that latitude and longitude have minimal impact on the prediction of solar radiation. Moreover, latitude and longitude are mainly used to determine the location of a specific site rather than directly influencing solar radiation levels [56-57].

Future research should focus on employing advanced techniques such as KNN, regression trees, boosting, and random forest models to improve the precision of predicting global solar radiation and the power output of PV systems. By exploring these models, researchers can contribute to more reliable and efficient solar energy utilization.

REFERENCES

[1] Y. Kassem, H. Camur, and O. a. M. Abughinda, "Solar Energy Potential and Feasibility Study of a 10MW Grid-connected Solar Plant in Libya,"

Engineering, Technology & Applied Science Research, vol. 10, no. 4, pp. 5358–5366, Aug. 2020, <https://doi.org/10.48084/etasr.3607>.

- [2] H. Camur, Y. Kassem, and E. Alessi, "A Techno-Economic Comparative Study of a Grid-Connected Residential Rooftop PV Panel: The Case Study of Nahr El-Bared, Lebanon," *Engineering, Technology & Applied Science Research*, vol. 11, no. 2, pp. 6956–6964, Apr. 2021, <https://doi.org/10.48084/etasr.4078>.
- [3] Y. Kassem, H. Gokcekus, I. A. A. Albakoush, and K. S. B. Abdullah, "Solar-Powered Solutions for the Water and Energy Shortage Problem: The Case Study of Nahr El Bared, Lebanon," *Engineering, Technology & Applied Science Research*, vol. 13, no. 3, pp. 10861–10869, Jun. 2023, <https://doi.org/10.48084/etasr.5858>.
- [4] Y. Kassem, H. Gökçekuş, A. Iravanian, and R. Gökçekuş, "Predictive suitability of renewable energy for desalination plants: the case of güzelyurt region in northern Cyprus," *Modeling Earth Systems and Environment*, vol. 8, no. 3, pp. 3657–3677, Sep. 2022, <https://doi.org/10.1007/s40808-021-01315-0>.
- [5] A. Suman, "Role of renewable energy technologies in climate change adaptation and mitigation: A brief review from Nepal," *Renewable and Sustainable Energy Reviews*, vol. 151, Nov. 2021, Art. no. 111524, <https://doi.org/10.1016/j.rser.2021.111524>.
- [6] M. Herrando, D. Elduque, C. Javierre, and N. Fueyo, "Life Cycle Assessment of solar energy systems for the provision of heating, cooling and electricity in buildings: A comparative analysis," *Energy Conversion and Management*, vol. 257, Apr. 2022, Art. no. 115402, <https://doi.org/10.1016/j.enconman.2022.115402>.
- [7] Y. Kassem, H. Çamur, and R. A. F. Aateg, "Exploring Solar and Wind Energy as a Power Generation Source for Solving the Electricity Crisis in Libya," *Energies*, vol. 13, no. 14, Jan. 2020, Art. no. 3708, <https://doi.org/10.3390/en13143708>.
- [8] Y. Kherbiche, N. Ihaddadene, R. Ihaddadene, F. Hadji, J. Mohamed, and A. H. Beghidja, "Solar Energy Potential Evaluation. Case of Study: M'Sila, an Algerian Province," *International Journal of Sustainable Development and Planning*, vol. 16, no. 8, pp. 1501–1508, Dec. 2021, <https://doi.org/10.18280/ijstdp.160811>.
- [9] Y. Kassem and A. A. Othman, "Selection of most relevant input parameters for predicting photovoltaic output power using machine learning and quadratic models," *Modeling Earth Systems and Environment*, vol. 8, no. 4, pp. 4661–4686, Nov. 2022, <https://doi.org/10.1007/s40808-022-01413-7>.
- [10] V. Demir and H. Citakoglu, "Forecasting of solar radiation using different machine learning approaches," *Neural Computing and Applications*, vol. 35, no. 1, pp. 887–906, Jan. 2023, <https://doi.org/10.1007/s00521-022-07841-x>.
- [11] O. Kisi, M. Alizamir, S. Trajkovic, J. Shiri, and S. Kim, "Solar Radiation Estimation in Mediterranean Climate by Weather Variables Using a Novel Bayesian Model Averaging and Machine Learning Methods," *Neural Processing Letters*, vol. 52, no. 3, pp. 2297–2318, Dec. 2020, <https://doi.org/10.1007/s11063-020-10350-4>.
- [12] B. Belmahdi, M. Louzazni, and A. El Bouardi, "Comparative optimization of global solar radiation forecasting using machine learning and time series models," *Environmental Science and Pollution Research*, vol. 29, no. 10, pp. 14871–14888, Feb. 2022, <https://doi.org/10.1007/s11356-021-16760-8>.
- [13] S. Banerjee *et al.*, "Machine Learning approach to Predict net radiation over crop surfaces from global solar radiation and canopy temperature data," *International Journal of Biometeorology*, vol. 66, no. 12, pp. 2405–2415, Dec. 2022, <https://doi.org/10.1007/s00484-022-02364-5>.
- [14] A. Sohani, S. Hoseinzadeh, S. Samiezadeh, and I. Verhaert, "Machine learning prediction approach for dynamic performance modeling of an enhanced solar still desalination system," *Journal of Thermal Analysis and Calorimetry*, vol. 147, no. 5, pp. 3919–3930, Mar. 2022, <https://doi.org/10.1007/s10973-021-10744-z>.
- [15] J. P. de Amorim Neto *et al.*, "Thermal behavior estimation of a solar wall operated by TiO₂ nanofluids using several machine learning models," *Journal of the Brazilian Society of Mechanical Sciences and Engineering*, vol. 44, no. 4, Mar. 2022, Art. no. 128, <https://doi.org/10.1007/s40430-022-03425-x>.

- [16] E. García-Cuesta, R. Aler, D. del Pózo-Vázquez, and I. M. Galván, "A combination of supervised dimensionality reduction and learning methods to forecast solar radiation," *Applied Intelligence*, vol. 53, no. 11, pp. 13053–13066, Jun. 2023, <https://doi.org/10.1007/s10489-022-04175-y>.
- [17] P. Verma and S. Patil, "A Machine Learning Approach and Methodology for Solar Radiation Assessment Using Multispectral Satellite Images," *Annals of Data Science*, vol. 10, no. 4, pp. 907–932, Aug. 2023, <https://doi.org/10.1007/s40745-021-00352-x>.
- [18] R. Janković, I. Mihajlović, N. Štrbac, and A. Amelio, "Machine learning models for ecological footprint prediction based on energy parameters," *Neural Computing and Applications*, vol. 33, no. 12, pp. 7073–7087, Jun. 2021, <https://doi.org/10.1007/s00521-020-05476-4>.
- [19] E. Ofori-Ntow Jr., Y. Y. Ziggah, M. J. Rodrigues, and S. Relvas, "A New Long-Term Photovoltaic Power Forecasting Model Based on Stacking Generalization Methodology," *Natural Resources Research*, vol. 31, no. 3, pp. 1265–1287, Jun. 2022, <https://doi.org/10.1007/s11053-022-10058-3>.
- [20] R. Muhammad Ehsan, S. P. Simon, and P. R. Venkateswaran, "Day-ahead forecasting of solar photovoltaic output power using multilayer perceptron," *Neural Computing and Applications*, vol. 28, no. 12, pp. 3981–3992, Dec. 2017, <https://doi.org/10.1007/s00521-016-2310-z>.
- [21] M. K. Park, J. M. Lee, W. H. Kang, J. M. Choi, and K. H. Lee, "Predictive model for PV power generation using RNN (LSTM)," *Journal of Mechanical Science and Technology*, vol. 35, no. 2, pp. 795–803, Feb. 2021, <https://doi.org/10.1007/s12206-021-0140-0>.
- [22] A. Kumar, M. Rizwan, and U. Nangia, "A Hybrid Intelligent Approach for Solar Photovoltaic Power Forecasting: Impact of Aerosol Data," *Arabian Journal for Science and Engineering*, vol. 45, no. 3, pp. 1715–1732, Mar. 2020, <https://doi.org/10.1007/s13369-019-04183-0>.
- [23] I. Arora, J. Gambhir, and T. Kaur, "Data Normalisation-Based Solar Irradiance Forecasting Using Artificial Neural Networks," *Arabian Journal for Science and Engineering*, vol. 46, no. 2, pp. 1333–1343, Feb. 2021, <https://doi.org/10.1007/s13369-020-05140-y>.
- [24] D. Shah, K. Patel, and M. Shah, "Prediction and estimation of solar radiation using artificial neural network (ANN) and fuzzy system: a comprehensive review," *International Journal of Energy and Water Resources*, vol. 5, no. 2, pp. 219–233, Jun. 2021, <https://doi.org/10.1007/s42108-021-00113-9>.
- [25] E. Dikmen, M. Ayaz, H. H. Ezen, E. U. Küçüksille, and A. Ş. Şahin, "Estimation and optimization of thermal performance of evacuated tube solar collector system," *Heat and Mass Transfer*, vol. 50, no. 5, pp. 711–719, May 2014, <https://doi.org/10.1007/s00231-013-1282-0>.
- [26] E. M. Natsheh, A. R. Natsheh, and A. H. Albarbar, "An automated tool for solar power systems," *Applied Solar Energy*, vol. 50, no. 4, pp. 221–227, Oct. 2014, <https://doi.org/10.3103/S0003701X14040094>.
- [27] B. Ihya, A. Mechaqrane, R. Tadili, and M. N. Bargach, "Prediction of hourly and daily diffuse solar fraction in the city of Fez (Morocco)," *Theoretical and Applied Climatology*, vol. 120, no. 3, pp. 737–749, May 2015, <https://doi.org/10.1007/s00704-014-1207-y>.
- [28] E. F. Alsina, M. Bortolini, M. Gamberi, and A. Regattieri, "Artificial neural network optimisation for monthly average daily global solar radiation prediction," *Energy Conversion and Management*, vol. 120, pp. 320–329, Jul. 2016, <https://doi.org/10.1016/j.enconman.2016.04.101>.
- [29] C. G. Ozoegwu, "Artificial neural network forecast of monthly mean daily global solar radiation of selected locations based on time series and month number," *Journal of Cleaner Production*, vol. 216, pp. 1–13, Apr. 2019, <https://doi.org/10.1016/j.jclepro.2019.01.096>.
- [30] V. Sivamadhavi and R. S. Selvaraj, "Prediction of monthly mean daily global solar radiation using Artificial Neural Network," *Journal of Earth System Science*, vol. 121, no. 6, pp. 1501–1510, Dec. 2012, <https://doi.org/10.1007/s12040-012-0235-1>.
- [31] S. Dhillon, C. Madhu, D. Kaur, and S. Singh, "A Solar Energy Forecast Model Using Neural Networks: Application for Prediction of Power for Wireless Sensor Networks in Precision Agriculture," *Wireless Personal Communications*, vol. 112, no. 4, pp. 2741–2760, Jun. 2020, <https://doi.org/10.1007/s11277-020-07173-w>.
- [32] M. Thangavelu, V. J. Parthiban, D. Kesavaraman, and T. Murugesan, "Forecasting of solar radiation for a cleaner environment using robust machine learning techniques," *Environmental Science and Pollution Research*, vol. 30, no. 11, pp. 30919–30932, Mar. 2023, <https://doi.org/10.1007/s11356-022-24321-w>.
- [33] J. R. Trapero, N. Kourentzes, and A. Martin, "Short-term solar irradiation forecasting based on Dynamic Harmonic Regression," *Energy*, vol. 84, pp. 289–295, May 2015, <https://doi.org/10.1016/j.energy.2015.02.100>.
- [34] A. K. Abdourazak, A. Souad, Z. Driss, and I. A. Ibrahim, "Forecasting Direct Normal Irradiation at Djibouti Using Artificial Neural Network," *International Journal of Energy and Power Engineering*, vol. 11, no. 4, pp. 393–396, Mar. 2017.
- [35] I. Belhaj and O. E. Fatni, "A Benchmark of Statistical Models for Forecasting Monthly Direct Normal Irradiation (DNI) for the Region of Ouarzazate Morocco," *International Journal of Renewable Energy Research (IJRER)*, vol. 9, no. 1, pp. 108–117, Mar. 2019.
- [36] I. Belhaj, O. E. Fatni, S. Barhmi, and E. H. Saidi, "A direct normal irradiation forecasting model based on," *Revue des Energies Renouvelables*, vol. 19, no. 1, pp. 21–28, 2016.
- [37] C. Zhang, Z. Yan, C. Ma, and X. Xu, "Prediction of Direct Normal Irradiation Based on CNN-LSTM Model," in *Proceedings of the 2020 5th International Conference on Multimedia Systems and Signal Processing*, New York, NY, USA, Apr. 2020, pp. 74–80, <https://doi.org/10.1145/3404716.3404719>.
- [38] Y. Kassem and H. Gökçekuş, "Do quadratic and Poisson regression models help to predict monthly rainfall?," presented at the 2nd International Conference on the Environment Survival and Sustainability (ESS 2019), Nicosia, North Cyprus, Oct. 2019, vol. 215, pp. 288–318, <https://doi.org/10.5004/dwt.2021.26397>.
- [39] A. Irvanian, Y. Kassem, and H. Gökçekuş, "Stress-strain behavior of modified expansive clay soil: experimental measurements and prediction models," *Environmental Earth Sciences*, vol. 81, no. 4, Feb. 2022, Art. no. 107, <https://doi.org/10.1007/s12665-022-10229-8>.
- [40] Y. Kassem, H. Gökçekuş, and A. A. S. Mosbah, "Prediction of monthly precipitation using various artificial models and comparison with mathematical models," *Environmental Science and Pollution Research*, vol. 30, no. 14, pp. 41209–41235, Mar. 2023, <https://doi.org/10.1007/s11356-022-24912-7>.
- [41] K. E. ArunKumar, D. V. Kalaga, Ch. M. S. Kumar, M. Kawaji, and T. M. Brenza, "Forecasting of COVID-19 using deep layer Recurrent Neural Networks (RNNs) with Gated Recurrent Units (GRUs) and Long Short-Term Memory (LSTM) cells," *Chaos, Solitons & Fractals*, vol. 146, May 2021, Art. no. 110861, <https://doi.org/10.1016/j.chaos.2021.110861>.
- [42] Y. Zheng, W. Zhang, J. Xie, and Q. Liu, "A Water Consumption Forecasting Model by Using a Nonlinear Autoregressive Network with Exogenous Inputs Based on Rough Attributes," *Water*, vol. 14, no. 3, Jan. 2022, Art. no. 329, <https://doi.org/10.3390/w14030329>.
- [43] V. Nourani, Ö. Kisi, and M. Komasi, "Two hybrid Artificial Intelligence approaches for modeling rainfall-runoff process," *Journal of Hydrology*, vol. 402, no. 1, pp. 41–59, May 2011, <https://doi.org/10.1016/j.jhydrol.2011.03.002>.
- [44] Y. Kassem and M. H. A. Abdalla, "Modeling predictive suitability to identify the potential of wind and solar energy as a driver of sustainable development in the Red Sea state, Sudan," *Environmental Science and Pollution Research*, vol. 29, no. 29, pp. 44233–44254, Jun. 2022, <https://doi.org/10.1007/s11356-022-19062-9>.
- [45] J. Dekker, M. Nthontho, S. Chowdhury, and S. P. Chowdhury, "Investigating the effects of solar modelling using different solar irradiation data sets and sources within South Africa," *Solar Energy*, vol. 86, no. 9, pp. 2354–2365, Sep. 2012, <https://doi.org/10.1016/j.solener.2012.05.007>.
- [46] A. K. Yadav, H. Malik, and S. S. Chandel, "Selection of most relevant input parameters using WEKA for artificial neural network based solar radiation prediction models," *Renewable and Sustainable Energy Reviews*, vol. 31, pp. 509–519, Mar. 2014, <https://doi.org/10.1016/j.rser.2013.12.008>.

- [47] S. Hussain and A. A. Alili, "A pruning approach to optimize synaptic connections and select relevant input parameters for neural network modelling of solar radiation," *Applied Soft Computing*, vol. 52, pp. 898–908, Mar. 2017, <https://doi.org/10.1016/j.asoc.2016.09.036>.
- [48] A. A. Babatunde, S. Abbasoglu, and M. Senol, "Analysis of the impact of dust, tilt angle and orientation on performance of PV Plants," *Renewable and Sustainable Energy Reviews*, vol. 90, pp. 1017–1026, Jul. 2018, <https://doi.org/10.1016/j.rser.2018.03.102>.
- [49] Y. Kassem, H. Gökçekuş, and A. Güvensoy, "Techno-Economic Feasibility of Grid-Connected Solar PV System at Near East University Hospital, Northern Cyprus," *Energies*, vol. 14, no. 22, Jan. 2021, Art. no. 7627, <https://doi.org/10.3390/en14227627>.
- [50] A. Alver and Z. Kazan, "Prediction of full-scale filtration plant performance using artificial neural networks based on principal component analysis," *Separation and Purification Technology*, vol. 230, Jan. 2020, Art. no. 115868, <https://doi.org/10.1016/j.seppur.2019.115868>.
- [51] A. Gholamy, V. Kreinovich, and O. Kosheleva, "Why 70/30 or 80/20 Relation Between Training and Testing Sets: A Pedagogical Explanation," University of Texas at El Paso, El Paso, TX, USA, Departmental Technical Report, Feb. 2018.
- [52] N. Al-Rousan, H. Al-Najjar, and O. Alomari, "Assessment of predicting hourly global solar radiation in Jordan based on Rules, Trees, Meta, Lazy and Function prediction methods," *Sustainable Energy Technologies and Assessments*, vol. 44, Apr. 2021, Art. no. 100923, <https://doi.org/10.1016/j.seta.2020.100923>.
- [53] G. Notton, C. Voyant, A. Foulloy, J. L. Duchaud, and M. L. Nivet, "Some Applications of ANN to Solar Radiation Estimation and Forecasting for Energy Applications," *Applied Sciences*, vol. 9, no. 1, Jan. 2019, Art. no. 209, <https://doi.org/10.3390/app9010209>.
- [54] F. M. Lopes, H. G. Silva, R. Salgado, A. Cavaco, P. Canhoto, and M. Collares-Pereira, "Short-term forecasts of GHI and DNI for solar energy systems operation: assessment of the ECMWF integrated forecasting system in southern Portugal," *Solar Energy*, vol. 170, pp. 14–30, Aug. 2018, <https://doi.org/10.1016/j.solener.2018.05.039>.
- [55] M. Diagne, M. David, P. Lauret, J. Boland, and N. Schmutz, "Review of solar irradiance forecasting methods and a proposition for small-scale insular grids," *Renewable and Sustainable Energy Reviews*, vol. 27, pp. 65–76, Nov. 2013, <https://doi.org/10.1016/j.rser.2013.06.042>.
- [56] B. Babar, R. Graverson, and T. Boström, "Solar radiation estimation at high latitudes: Assessment of the CMSAF databases, ASR and ERA5," *Solar Energy*, vol. 182, pp. 397–411, Apr. 2019, <https://doi.org/10.1016/j.solener.2019.02.058>.
- [57] J. L. Kafka and M. A. Miller, "A climatology of solar irradiance and its controls across the United States: Implications for solar panel orientation," *Renewable Energy*, vol. 135, pp. 897–907, May 2019, <https://doi.org/10.1016/j.renene.2018.12.057>.